AIAA SciTech Forum
12-16 January 2026, Orlando, FL
AIAA SCITECH 2026 Forum

Mokotoff, P. R., and Cinar, G. (2026). Reliability and Performance Trade Studies for NASA's Subsonic Single Aft Engine Aircraft. AIAA SciTech 2026 Forum. American Institute of Aeronautics and Astronautics. https://doi.org/10.2514/6.2026-1710

10.2514/6.2026-1710

Reliability and Performance Trade Studies for NASA's Subsonic Single Aft Engine Aircraft

Paul R. Mokotoff* and Gokcin Cinar†
Department of Aerospace Engineering, University of Michigan, Ann Arbor, Michigan 48109

NASA's SUbsonic Single Aft eNgine (SUSAN) Aircraft is regarded as a transformational aircraft concept to make commercial flight more efficient. Its series/parallel-partial hybrid propulsion architecture, with sixteen electric propulsors (EP) and an aft turbofan engine, was previously sized for weight and performance objectives without a quantitative safety assessment. To fill this gap, an integrated performance–reliability framework was developed to evaluate certification-relevant "k-EP inoperative" failure conditions under FAA Part 25.1309 regulations by: 1) embedding cable weights and losses into a graph-based propulsion system analysis; and 2) deriving minimal cut sets directly from a propulsion system architecture matrix. Five failure modes (1-, 2-, 4-, 8-, and 16-EP inoperative) are analyzed on SUSAN's baseline propulsion architecture and four others with redundant electric generator–motor cross-connection schemes. Relative to the baseline, added redundancy increases block fuel by at most 1.5% but, depending on the failure mode, improves system-level failure intensity by up to *seven orders of magnitude*. These results enable identification of Pareto-optimal system architectures for two objectives: 1) minimum fuel burn; and 2) largest excess safety margin. In addition, the formulation and analyses used for SUSAN enable transparent reuse in future safety trade studies for electrified transport aircraft.

I. Introduction

NASA's Electrified Aircraft Propulsion research develops next-generation aircraft concepts for more efficient flight. One example is the SUbsonic Single Aft eNgine (SUSAN) aircraft [1], depicted in Fig. 1, which is designed to fly 4,630 km and 180 passengers (weighing 100 kg each) while cruising at Mach 0.775 [2]. Its series/parallel-partial hybrid propulsion architecture and advanced electrification technologies save 8.4% and 9.6% fuel on 1,390 and 1,850 km missions, respectively, relative to a Boeing 737-800 Max re-designed for the same 4,630 km design range [2].

Fig. 1 NASA's SUSAN aircraft concept [1].

*Graduate Research Assistant, Department of Aerospace Engineering, University of Michigan, Ann Arbor, Michigan 48109, AIAA Student Member.

†Assistant Professor, Department of Aerospace Engineering, University of Michigan, Ann Arbor, Michigan 48109, AIAA Senior Member.

SUSAN's system and subsystem designs have been significant research thrusts at NASA for many years. Initial studies on SUSAN involved exploring four different airframe and propulsion architecture combinations [3], which included either counter-rotating propfans or distributed electric propulsors on the wing and counter-rotating propfans or a ducted turbofan aft of the fuselage. Ultimately, the aft turbofan with distributed electric propulsors was down-selected for further design because it exhibited the largest fuel burn savings on a 1,390 km economy mission and the greatest thrust specific fuel consumption reduction among the configurations evaluated. Further studies refined SUSAN's design, as comprehensively summarized by Jansen et al. [4].

After selecting the system architecture, research efforts focused on the aft engine design and distributed propulsor placement. Mirhashemi et al. [5] designed the aft engine to be a ducted turbofan without any additional power-siphoning turbines beyond the low-pressure turbine. Natural gas was considered as an alternative to kerosene for powering the turbofan; its larger lower heating value relative to kerosene enabled the turbofan engine to be downsized by 3%. Then, Machado et al. [6] performed detailed aerodynamic analyses to explore whether the distributed electric propulsors should be placed over the wing, under the wing, or aft of the wing's trailing edge. They also began integrating the aft engine with the fuselage, utilizing shape optimization to ensure a smooth flow into the diffuser.

At the same time, other research explored optimal thermal management and electrical system designs. Heersema and Jansen [7] explored different thermal management system designs, including traditional liquid-air heat exchangers and oscillating heat pipes. Haglage et al. [8] explored different electrical system architectures to connect the generators and motors together. Ultimately, a 16 bus system was selected to limit over-sizing the components and provide a failure mitigation strategy rooted in the distributed electric propulsion system's inherent redundancy.

Then, to further enhance SUSAN's efficiency, advanced technologies were included in the design. Lynde et al. [9] reshaped the upper surface of SUSAN's airfoils on the main wing to reduce the drag coefficient by 0.019. Machado et al. [10] compared the benefits of including distributed electric propulsors with mail-slot nacelles under each wing relative to a configuration with high-bypass turbofan engines. The distributed electric propulsors offered a 1.3% shaft power savings along with a 22% drag reduction for the same net thrust as the turbofan configuration.

The novelty of SUSAN's propulsion system required additional efforts to ensure airworthiness and a path to certification. Denham and Jansen [11] explored the regulatory barriers to certifying SUSAN, especially those pertaining to the electrified propulsion system. Flight performance requirements, such as the ability to takeoff and climb with an inoperative turbofan engine, were also considered. As a result, a single-use backup battery was added to power the distributed electric propulsion system during a turbofan engine failure. Additionally, they cite that the inherent redundancy within SUSAN's distributed electric propulsion system prevents any single-point propulsion system failures from occurring. In a follow-up study, Denham et al. [12] designed diversion mission profiles for SUSAN under different propulsion system failure modes such as an inoperative turbofan or electric propulsor during takeoff and cruise.

II. Objective: Performance-Reliability Framework and Trade Studies

Prior system design studies on SUSAN assumed that redundancy in the distributed electric propulsion system renders the aircraft as "safe" to fly, particularly since single point failures were mitigated. As a result, SUSAN's subsystem design studies only considered performance and weight objectives without quantitatively analyzing system safety. However, such analysis is necessary for certification, along with identifying the propulsion system's primary failure modes and conducting a reliability analysis to ensure that it meets the criteria delineated in FAA Part 25 regulations [13], the federal statutes governing transport aircraft certification. These regulations were developed for conventional aircraft concepts and must be updated to accommodate nascent electrified aircraft designs.

To enhance SUSAN's prior system design studies, this research establishes a performance-reliability framework to assess system-level trade studies on SUSAN's performance and safety. These trades are examined on SUSAN's baseline propulsion architecture and four others with redundant electric generator-motor cross-connection schemes. System-level performance (fuel burn and component weights) is assessed by integrating each propulsion system into SUSAN and sizing it under the same design requirements and mission profile. System-level safety (failure intensity and minimal cut sets) is assessed using a Fault Tree Analysis (FTA) to identify the minimum number of generators and motors that may fail before losing a critical amount of thrust. Due to the lack of certification regulations for future aircraft concepts, particularly engine inoperative conditions, multiple failure scenarios are considered to account for the uncertainty in future safety requirements. Pareto Frontiers are generated to identify optimal propulsion system architectures that either minimize fuel burn or maximize the required safety margin.

A. Contributions

Four key contributions are made in this paper:

1) An integrated graph-based propulsion system analysis with explicit cable losses/weights to model SUSAN;
2) A FTA formulation directly from propulsion system architecture matrices to evaluate k-EP inoperative scenarios;
3) Quantified performance–safety tradeoffs across SUSAN's baseline and four redundant propulsion system architectures; and
4) Identification of certification-relevant architectures under FAA Part 25.1309 regulations.

B. Paper Structure

The remainder of the paper is structured as follows. Section III describes how SUSAN was modeled, along with the methodology and assumptions made in the performance and safety assessments. Section IV defines the trade study and proposes redundant system architectures to be analyzed. Then, Pareto Frontiers are generated to identify the tradeoffs between system-level performance and safety. Section V concludes the paper and provides areas for future investigation.

III. Technical Approach

First, the modeling methodology and assumptions to evaluate SUSAN's system-level performance are described in Section III.A. Then, the FTA methodology and assumptions for the system-level safety analysis are explained in Section III.B.

A. Sizing and Performance Analysis

SUSAN was modeled using the Future Aircraft Sizing Tool (FAST) [14], a MATLAB-based open-source aircraft sizing tool for early-phase conceptual design. The parameters used to model SUSAN are listed in Appendix V.A.

One of FAST's distinguishing features is its graph-based propulsion system analysis framework [15], which represents the propulsion system as a directed graph and encodes it in a machine readable manner. This flexible framework enables the engineer to easily change component connections and add redundancy into the propulsion system architecture. To simplify the propulsion system analysis in this study, all batteries and electrical components (buses, circuit breakers, contactors, relays, etc.) *except cables* were neglected. Instead, these components were accounted for by allocating a constant 9,178 kg to an electrified aircraft propulsion weight group (herinafter referred to as "EAP Weight"), consistent with prior system-level analyses performed [16]. The resultant propulsion system architecture used in the analysis is illustrated in Fig. 2. Fans 1 through 16 are powered by the distributed electric propulsion system; Fan 17 is the one installed on the aft turbofan engine.

In prior SUSAN design studies [16], only the turbofan engine, generators, and motors were modeled. However, system-level performance is greatly impacted by the cables connecting the generators and motors – redundant connections require more cables to be installed on the aircraft, thus increasing the structural weight required to support the airframe and propulsion system. Therefore, this study includes the cable weights and efficiencies in the propulsion system model.

Table 1 lists the electrical component performance parameters used in this study. Each of the values in the table are the "nominal" values predicted by Haglage et al. [8] and were also used by Chau and Duensing [2] while they developed SUSAN's propulsion system model.

Table 1 Electrical component performance parameters.

Component	Power-Weight Ratio	Efficiency
Electric Generator	25 kW/kg	99.0%
Electric Motor	20 kW/kg	98.5%
Cables	2 kg/m/MW	0.040% loss/m

To determine each cable's weight and overall efficiency, its length must be estimated. This was accomplished by digitizing the "SUSAN Electrofan power system diagram" in Fig. 3 (shown as Fig. 5 in Ref. [2]) and computing the total cable length from the generators to each motor. Since there is no reference length in the schematic, the digitizer was calibrated using the wingspan provided by Chau and Duensing [2].

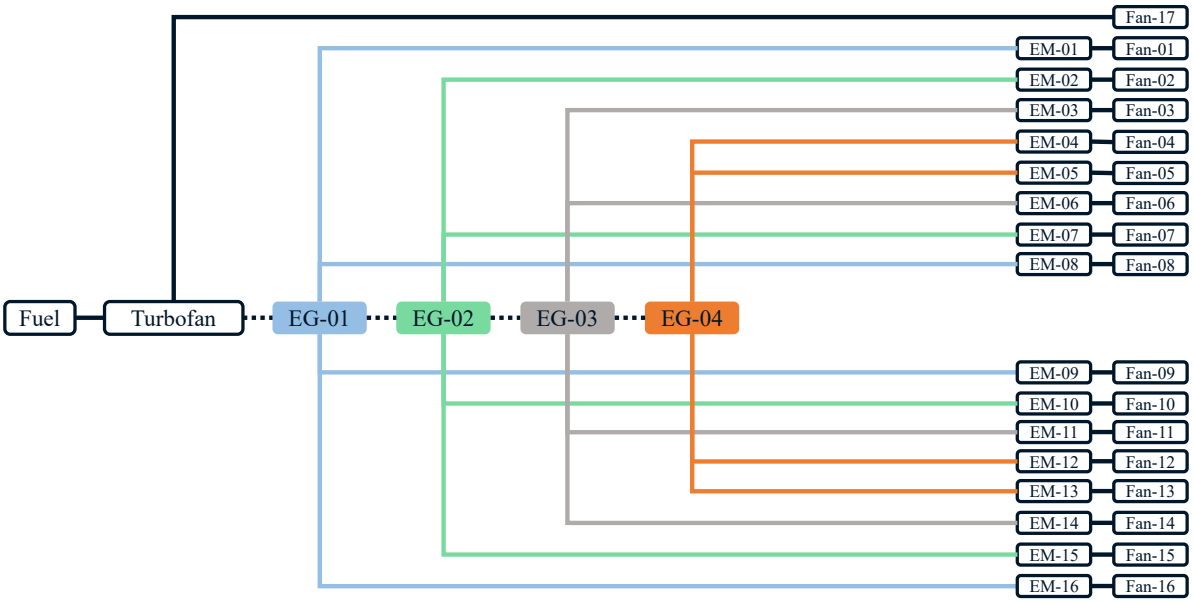

Fig. 2 SUSAN's simplified propulsion architecture for analysis in FAST. The turbofan engine connects to all generators (EGs), illustrated by the dashed line.

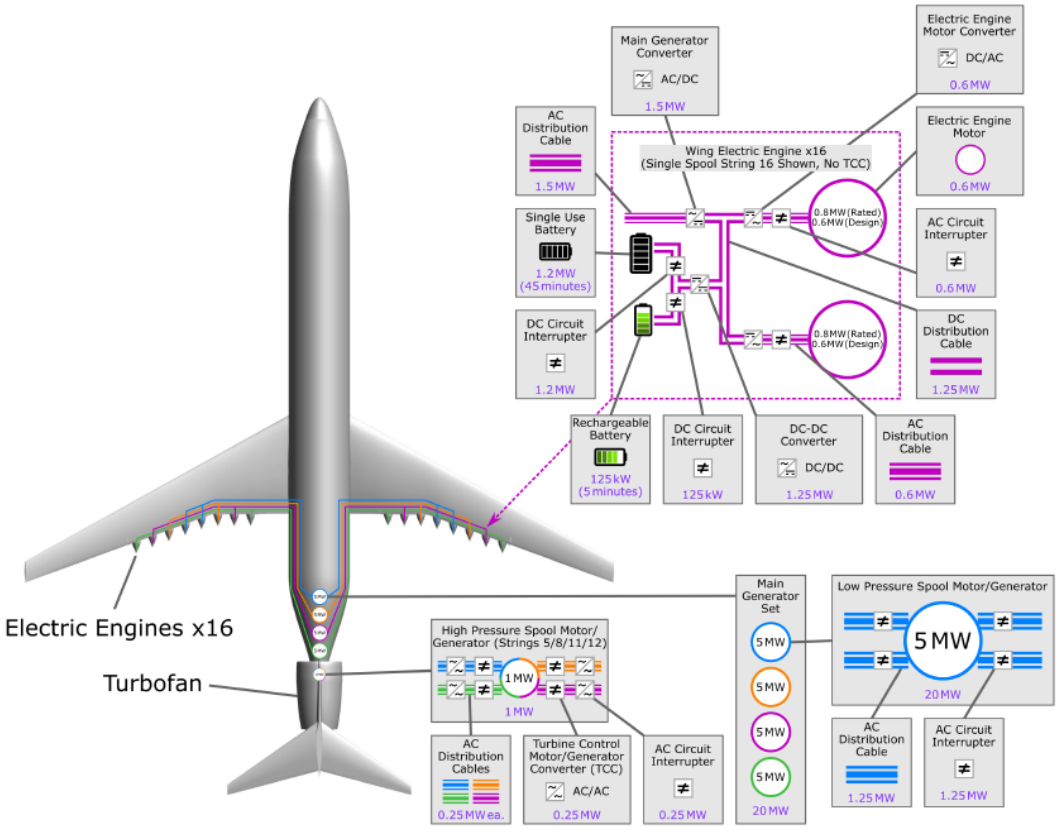

Fig. 3 Schematic digitized to estimate the cable lengths, adapted from Ref. [2].

Existing SUSAN literature does not contain any information about the exact generator placement. However, prior studies [2, 8, 17] all refer to the same schematic as Fig. 3, which places the generators consecutively along the fuselage centerline in the tailcone. This is likely done to minimize the weight of the gearboxes and mechanical couplings required to spin the generators from the turbofan engine. Thus, each generator's position was assumed to be the center of each circle on the schematic.

As shown in Fig. 2, Generators 1 and 4 are the closest and farthest from the turbofan engine, respectively; Motors 1 and 16 are the most port and starboard positions along the wingspan, respectively. Using these component positions while digitizing Fig. 3, the cable lengths were computed, and are included in Appendix V.B. The cable lengths were multiplied by the nominal loss per unit length to compute the overall efficiency of each cable, as listed in Tab. 2.

Table 2 Estimated cable efficiency after digitizing the propulsion system schematic (all in %).

	Generator 1	**Generator 2**	**Generator 3**	**Generator 4**
Motors 1/16	99.25	99.28	99.30	99.31
Motors 2/15	99.30	99.32	99.35	99.36
Motors 3/14	99.34	99.37	99.39	99.41
Motors 4/13	99.39	99.41	99.44	99.45
Motors 5/12	99.43	99.45	99.48	99.49
Motors 6/11	99.47	99.49	99.52	99.54
Motors 7/10	99.51	99.53	99.56	99.57
Motors 8/9	99.55	99.57	99.60	99.61

After collecting data to model the propulsion system, SUSAN was calibrated in FAST while flying the design mission profile established in a prior study [16]. This was accomplished by imposing calibration factors on the airframe weight and fuel flow rate to match the MTOW and fuel burn for a 4,630 km mission with reserves. Extra attention was focused on ensuring that the fuel burn closely matched the value from literature because it will be used in the upcoming trade studies in Section IV. Table 3 lists the calibration factors and Tab. 4 compares the MTOW and fuel burn output by FAST relative to the same values provided in literature.

Table 3 Calibration factors applied to model SUSAN in FAST.

Calibration Factor	**Value**
Airframe Weight	1.094
Fuel Flow	0.950

The tuned calibration factors are within 10% of unity, indicating that SUSAN's behavior is not significantly altered by the model calibration. After calibrating, the resultant SUSAN model in FAST returns MTOW and fuel burn values that closely match those provided in literature [2]. This validates SUSAN's model developed in FAST, and serves as a baseline for the trade studies conducted in Section IV.

Table 4 Weight comparison between the SUSAN model in FAST and literature (all weights in kg).

Weight	**FAST Model**	**Literature**	**Percent Error**
MTOW	86,456	86,586	-0.15%
Fuel Burn	13,706	13,791	-0.61%
OEW	54,008	54,862	-1.56%

B. System Safety Analysis

To analyze system safety, a FTA was used to derive minimal cut sets – combinations of the fewest component failures that can simultaneously occur to result in a system failure [18, 19] – within the baseline and redundant propulsion system architectures. This research assesses failure modes pertaining to SUSAN's distributed electric propulsion system. Since certification regulations have yet to be developed for advanced aircraft concepts, five failure modes were considered, consisting of a minimum of either 1-, 2-, 4-, 8-, or 16-electric propulsor failures (referred to as "k-EP failure modes/scenarios" hereafter). Each failure mode is characterized by a *minimum* number of component failures because one component failure can result in the loss of many electric propulsors, allowing multiple proposed failure modes to be realized. For example, a generator failure in SUSAN's baseline propulsion system architecture causes four electric propulsors to fail, satisfying the minimum criteria for three of the five proposed failure modes. This next section explores the failure rates assigned to the components in SUSAN's propulsion system, the FTA analysis algorithm developed, and an FTA demonstration on a simple system architecture.

1. Component Failure Rates

For the system-level studies performed in this work, only generator and motor failures were considered in the safety analysis. Other electrical components (batteries, buses, circuit breakers, etc.) *including cables* were assumed to be fully functional and disregarded from the safety analysis. The same assumption was applied to the aft turbofan engine and fans in the distributed electric propulsion system.

Each component's "Applied Failure Rate", listed in Tab. 5, was estimated by multiplying its "Baseline Failure Rate" by an "Applied Environmental Factor", as previously done by Darmstadt et al. [20]. Since the "Baseline Failure Rate" was identified from failure rates of similar components, the "Applied Environmental Factor" serves to conservatively estimate a reasonable failure rate for state-of-the-art technologies, primarily due to a lack of technological maturity.

Table 5 Component failure rates and probabilities.

Component	Baseline Failure Rate (failures per 10^6 flight hours)	Applied Environmental Factor	Applied Failure Rate (failures per 10^6 flight hours)	Probability of Failure (per flight)
Electric Generator	13.00	10	130.0	7.52×10^{-4}
Electric Motor	9.24	10	92.4	5.35×10^{-4}

To remain consistent with practices established in SAE ARP4761A [18], the reliability, R_i, (or probability of success, P_{S_i}) is treated as a constant-intensity exponential distribution, provided in Eq. 1, where λ_i is the Applied Failure Rate from Tab. 5 and T is the exposure time, assumed to be the duration of SUSAN's main mission (fly 4,630 km), approximately 5.78 hours. Conversely, the unreliability, Q_i, (or probability of failure, P_{F_i}) is the probability that the component is not reliable, as listed in Eq. 2. Component reliability and unreliability are complementary events ($R_i + Q_i = 1$), allowing Q_i to be defined as the complement of R_i.

$$R_i = P_{S_i} = e^{\lambda_i T} \tag{1}$$

$$Q_i = P_{F_i} = 1 - e^{\lambda_i T} \tag{2}$$

Assuming that each failure is a rare event ($\lambda_i T \ll 1$), then the component failure probability is approximated by Eq. 3 (a linearization of Eq. 2 about $\lambda_i T = 0$).

$$Q_i = P_{F_i} \approx \lambda_i T \tag{3}$$

This probability is measured as the "probability of failure per flight," as indicated in the final column of Tab. 5, and is input into the FTA.

2. Fault Tree Analysis Algorithm

In the FTA, minimal cut sets, C_j, are obtained by traversing a graph of the propulsion system architecture to identify all combinations of component failures that will result in one of the aforementioned failure modes occurring. This is

achieved through a k-out-of-n gate, which defines a propulsion system failure as k electric propulsors failing out of n electric propulsors available. Assuming statistical independence among propulsion system failures, the system failure probability per flight is approximated by Eq. 4.

$$Q_{\text{sys}} \approx \sum_{j} \prod_{i \in C_j} Q_i \tag{4}$$

To align with guidance provided in the FAA Advisory Circular 25.1309-1B [21], the FTA returns a failure intensity per flight hour (λ_{sys}) by dividing the system failure probability by the exposure time, as listed in Eq. 5.

$$\lambda_{\text{sys}} = Q_{\text{sys}}/T \tag{5}$$

The FTA algorithm to compute the system failure intensity is defined in Algorithm 1. This function runs using the propulsion system architecture matrix (A) input to FAST, and each component's failure probability from Tab. 5.

Algorithm 1 Fault tree analysis.

FAULT TREE ANALYSIS
Input A, Component Failure Probabilities, and the first component to analyze
Check for an internal failure mode at the current component and remember it, if available
Find all possible failures using `COMPUTE MINIMAL CUT SET`, starting at the current component
Use the Idempotent Law to simplify the possible failures among the minimal cut sets
Use the Law of Absorption to simplify the remaining failures among the minimal cut sets
Apply failure probabilities to all failed components
Compute the failure intensity (per flight hour)
return Failure Intensity and Minimal Cut Sets
end FAULT TREE ANALYSIS

COMPUTE MINIMAL CUT SET
Input A and the current component being analyzed
Use A to find all children components that power the current component
for all children components **do**
    Run `COMPUTE MINIMAL CUT SET` to find their possible failure modes
end for
Enumerate the failure modes found in the **for** loop
Use the Idempotent Law to simplify the enumerated failures
Use the Law of Absorption to simplify the remaining failures
return Enumerated Failures
end COMPUTE MINIMAL CUT SET

The FTA algorithm operates as follows. Each branch of the propulsion system architecture is traversed to find a Boolean expression that represents all possible component failures leading to a system-level failure. Once these failures are identified, they are enumerated to account for all possible failure combinations. Since the set of enumerated failures is large and may contain duplicate events, the Boolean expressions are simplified using the Idempotent Law and Law of Absorption [22], listed in Eqs. 6 and 7, respectively.

$$\text{Idempotent Law:} \quad X \cap X = X \qquad X \cup X = X \tag{6}$$

$$\text{Law of Absorption:} \quad X \cap (X \cup Y) = X \qquad X \cup (X \cap Y) = X \tag{7}$$

Once the Boolean expressions are simplified, they are converted into mathematical expressions. Any Boolean `AND`, represented by $\cap$, is replaced with scalar multiplication. Conversely, any Boolean `OR`, represented by $\cup$, is replaced with scalar addition. Then, the component failure probabilities are substituted into the Boolean expression, allowing the failure intensity per flight hour to be attained.

3. Fault Tree Analysis Demonstration

To demonstrate the algorithm, a simple four-component system is used, as illustrated in Fig. 4. The architecture matrix representing the configuration is listed in Eq. 8 (refer to Ref. [15] for more information about these matrices). In this example, assume all component failure rates, λ_i, are 10^{-2} per flight hour and the exposure time, T, is one hour.

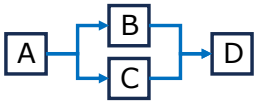

Fig. 4 Example system architecture for FTA algorithm.

$$A = \begin{bmatrix} 0 & 1 & 1 & 0 \\ 0 & 0 & 0 & 2 \\ 0 & 0 & 0 & 2 \\ 0 & 0 & 0 & 0 \end{bmatrix} \tag{8}$$

Aside from representing component connections, the values in each column of A also represent the number of components needed to fail before triggering the k-out-of-n gate. For example, Components B or C fail if one downstream component fails (Component A). However, Component D fails if two downstream components fail (both Components B and C). While trivial in this example, the encoding enables multiple failure modes to be considered with minimal adjustments to the propulsion system architecture matrix.

The FTA begins at Component D, the most upstream component, and its failure mode is remembered. Then, A is checked to find the components that flow into Component D, namely, Components B and C.

Component D will also fail if both Components B and C fail. Thus, the system-level failure probability is:

$$P(\text{fail}) = P(\text{D fail}) \cup [P(\text{B fail}) \cap P(\text{C fail})]$$

Next, Components B and C are searched recursively. For both Components B and C, their only input is Component A. Component B and C will fail either individually or if Component A fails. Thus, the probability that Components B and C fail are:

$$P(\text{B fail}) = P(\text{B fail}) \cup P(\text{A fail})$$
$$P(\text{C fail}) = P(\text{C fail}) \cup P(\text{A fail})$$

These failure modes cannot be simplified using the Idempotent Law or Law of Absorption, so they are returned as written. Then, they are input into the system-level failure probability expression:

$$\begin{aligned} P(\text{fail}) = \quad & P(\text{D fail}) \cup \\ & \{[P(\text{B fail}) \cup P(\text{A fail})] \cap \\ & [P(\text{C fail}) \cup P(\text{A fail})]\} \end{aligned}$$

Next, the failures are enumerated by expanding the `AND` operators ($\cap$) in the Boolean expression:

$$\begin{aligned} P(\text{fail}) = \quad & P(\text{D fail}) \cup \\ & [P(\text{B fail}) \cap P(\text{C fail})] \cup \\ & [P(\text{B fail}) \cap P(\text{A fail})] \cup \\ & [P(\text{C fail}) \cap P(\text{A fail})] \cup \\ & [P(\text{A fail}) \cap P(\text{A fail})] \end{aligned}$$

Using the Idempotent Law, any duplicated event is reduced from the Boolean expression. In this example, the failure of Component A is duplicated in the last term. The updated Boolean expression becomes:

$$\begin{aligned} P(\text{fail}) = \quad & P(\text{D fail}) \cup \\ & [P(\text{B fail}) \cap P(\text{C fail})] \cup \\ & [P(\text{B fail}) \cap P(\text{A fail})] \cup \\ & [P(\text{C fail}) \cap P(\text{A fail})] \cup \\ & P(\text{A fail}) \end{aligned}$$

Then, the Law of Absorption is used to eliminate redundant events. In this example, the failure of Component A also exists in the failure of Components B/A and Components C/A. After reducing, the Boolean expression is:

$$\begin{aligned} P(\text{fail}) = \quad & P(\text{D fail}) \cup \\ & [P(\text{B fail}) \cap P(\text{C fail})] \cup \\ & P(\text{A fail}) \end{aligned}$$

Lastly, the component-level failure probabilities are substituted into the fully reduced Boolean expression:

$$P(\text{fail}) = 10^{-2} + (10^{-2} \times 10^{-2}) + 10^{-2}$$

Evaluating the expression yields a system-level failure intensity of 2.01×10^{-2}/hr. The result is dominated by single-point failures of Components A or D (each 10^{-2}/hr). The redundant path through B and C contributes 10^{-4}/hr to the system-level failure intensity.

Since the exposure time is one hour, the system-level failure intensity is equal to the probability of failure. This is merely a coincidence and a result of selecting a convenient exposure time for the example.

IV. Performance-Reliability Trade Study

Using the performance and reliability analyses described in Section III, the baseline and four redundant propulsion system architectures were analyzed on SUSAN. The four redundant propulsion system architectures are illustrated in Appendix V.C and include the following configurations:

1) *Double Redundancy*: each motor is connected to two generators.
2) *Triple Redundancy*: each motor is connected to three generators.
3) *Quadruple Redundancy*: each motor is connected to all four generators.
4) *Double In(board), Triple Out(board)*: the eight outboard motors are connected to three generators and the eight inboard motors are connected to two generators.

In each redundant propulsion system architecture, the generators were sized to fully power eight motors, allowing them to operate at their rated power if one generator fails. If multiple generators fail, then the overall propulsion system performance is degraded because the motors can no longer operate at their rated power – this is standard for any abnormal in-flight scenario involving a propulsion system failure. The decision to increase each generator's size contrasts prior SUSAN design studies; the generators were previously sized to only power four motors [2].

First, system-level performance is assessed by comparing the fuel burn and component weights of each configuration in Section IV.A. Then, system-level safety is compared between configurations for the previously defined failure modes in Section III.B. Lastly, a Pareto Frontier illustrates the tradeoffs between system-level performance and safety in Section IV.C. A discussion reviews the tradeoffs between the baseline and redundant propulsion system architectures, selecting Pareto-optimal ones for each failure mode.

A. System Performance: Fuel Burn and Weight Breakdown

The weight breakdown in Tab. 6 reveals the MTOW and fuel burn increase for additional redundancy in the propulsion system architecture. In the worst case scenario (Quadruple Redundancy), there is a 1.5% fuel burn penalty. As expected, the cable and generator weights change the most – additional cables provide redundancy and the generators were resized to power eight motors (as opposed to four in the baseline configuration). The other aircraft components are

resized accordingly to accommodate the additional cable and generator weight. However, their impact on MTOW is negligible relative to that from the cables and generators.

Table 6 System-level weight breakdowns (all in kg). The percent difference relative to the baseline configuration is included in parenthesis for each redundant configuration.

Configuration	Baseline	Double	Double In, Triple Out	Triple	Quadruple
MTOW	86,456	87,912	88,260	88,518	89,131
	—	(+1.68%)	(+2.09%)	(+2.39%)	(+3.09%)
Fuel	13,706	13,815	13,841	13,860	13,907
	—	(+0.80%)	(+0.99%)	(+1.13%)	(+1.47%)
Airframe	37,582	37,678	37,698	37,712	37,744
	—	(+0.26%)	(+0.31%)	(+0.35%)	(+0.43%)
Engine	5,338	5,431	5,453	5,469	5,508
	—	(+1.73%)	(+2.15%)	(+2.45%)	(+3.19%)
Electric Generators	652	1,327	1,332	1,336	1,346
	—	(+103.37%)	(+104.17%)	(+104.77%)	(+106.21%)
Electric Motors	803	816	820	822	828
	—	(+1.68%)	(+2.09%)	(+2.38%)	(+3.11%)
Cables	455	926	1,198	1,399	1,878
	—	(+103.35%)	(+163.00%)	(+207.29%)	(+312.64%)

Weight breakdowns are plotted in Fig. 5 to graphically represent the impacts of adding redundancy to the propulsion system architecture, revealing a more qualitative summary of the results. Fig. 5a includes all weight groups listed in Tab. 6, while Fig. 5b only includes the generator, motor, and cable weights, better revealing the impacts of adding redundant generator-motor connections and doubling each generator's size. Recall that the "EAP weight" block was assumed to be a constant 9,178 kg and represents all of the systems on SUSAN's electrified propulsion system (batteries, buses, circuit breakers, etc.) *excluding cables*. Future work could involve sizing these other components, but is too granular for this system-level study.

The combined generator, motor, and cable weights in the redundant propulsion systems are approximately 1,150 to 2,140 kg heavier than the baseline. Besides the additional cables included, system performance is most impacted by the decision to size the generators to power eight motors. To accommodate additional generator failures, it is possible to size them to power 12 or 16 motors. However, any generator failure on SUSAN can be likened to an engine failure on a conventional aircraft, thus constituting an abnormal flight scenario and requiring a diversion to an alternate airport. The decision to size the generators to power eight motors can be further justified by considering conventional aircraft configurations with two, three, or four turbofan engines – a loss of one engine results in significantly degraded flight performance characteristics. Therefore, it is unrealistic to expect SUSAN to perform nominally during an abnormal flight scenario. Although the engineer may be tempted to over-size the generators to ensure maximum performance during abnormal scenarios, SUSAN's nominal performance during standard operations would be further degraded, requiring more fuel to fly as a result of the heavier generators.

Additionally, the presence of the distributed electric propulsion system allows SUSAN's performance to degrade more gracefully than a conventional turbofan aircraft. If one or two of SUSAN's electric propulsors fail, approximately 4-8% of its power available is lost. In contrast, an engine failure on a conventional turbofan aircraft causes 25-50% of its power available to be lost. Based on this argument, SUSAN can perform better in abnormal scenarios than conventional turbofan aircraft, further justifying why the generators do not need to be significantly over-sized.

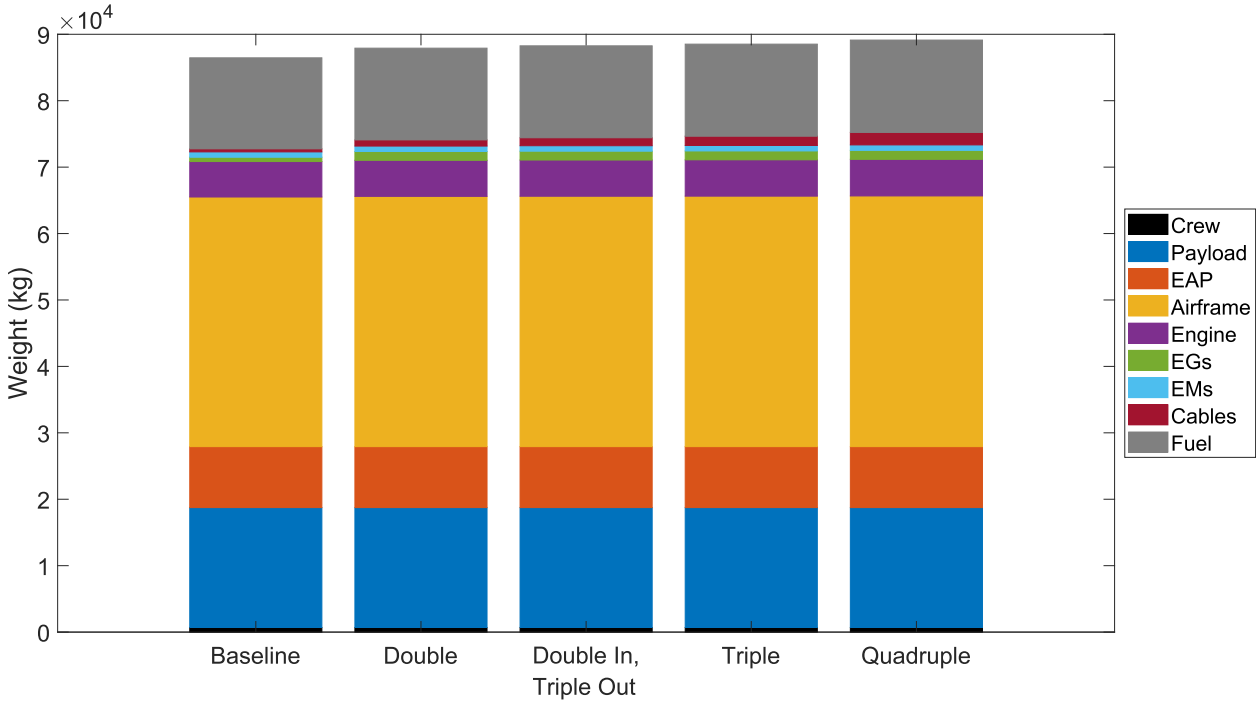

(a) System-level weights.

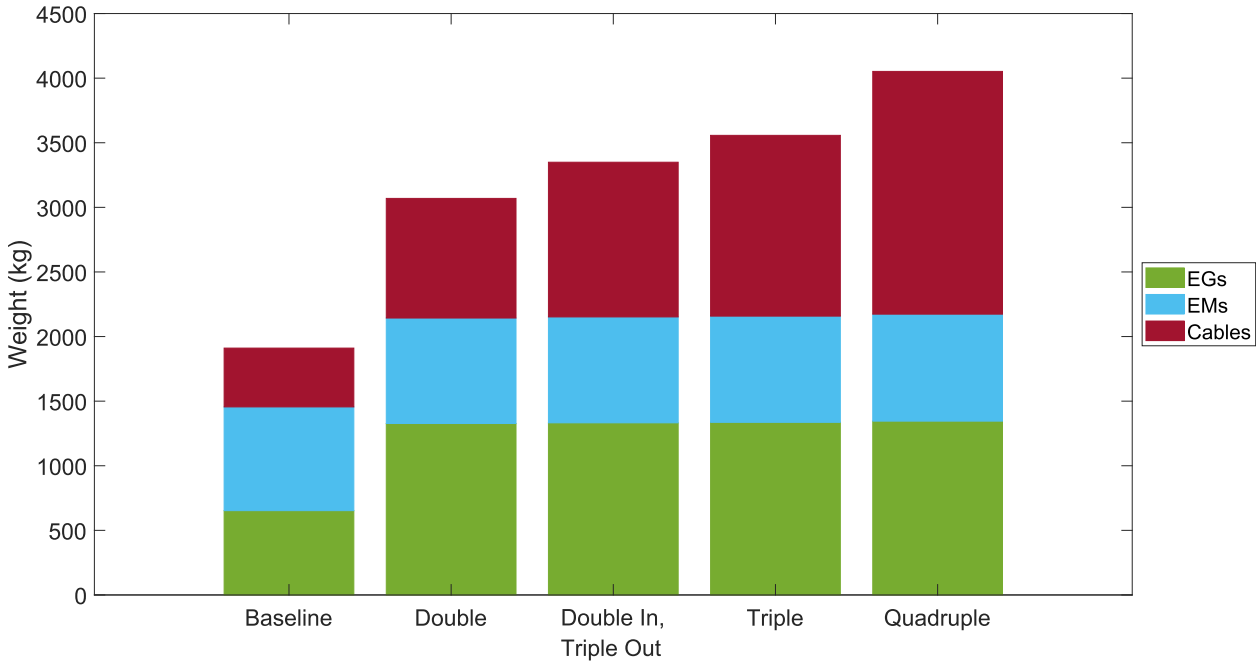

(b) Electrical component weights.

Fig. 5 Weight breakdowns for all configurations examined.

B. System Safety: Failure Intensity and Minimal Cut Sets

The system-level failure intensities in Tab. 7 illustrate the system safety improvements for increased redundancy in the propulsion system. Across each row, the failure intensity monotonically decreases as a result of adding more redundant connections in the propulsion system architecture. Down each column, the failure intensity monotonically decreases as a result of permitting more electric propulsors to fail before a system-level failure is triggered. Depending on the failure mode selected, the redundant system architectures may provide system safety improvements that span multiple orders of magnitude, as shown for the 2-, 4-, and 8-EP failure scenarios. However, other failure scenarios (1- and 16-EP) do not benefit from increased redundancy.

Table 7 Failure intensities (per flight hour) for each configuration under varying failure modes.

Failure Mode	Baseline	Double	Double In, Triple Out	Triple	Quadruple
1-EP	2.00×10^{-03}	1.50×10^{-03}	1.50×10^{-03}	1.50×10^{-03}	1.50×10^{-03}
2-EP	5.26×10^{-04}	6.12×10^{-06}	6.12×10^{-06}	5.93×10^{-06}	5.93×10^{-06}
4-EP	5.20×10^{-04}	1.96×10^{-07}	1.96×10^{-07}	3.20×10^{-10}	2.58×10^{-11}
8-EP	5.87×10^{-07}	1.96×10^{-07}	5.91×10^{-14}	5.53×10^{-14}	5.53×10^{-14}
16-EP	5.53×10^{-14}	5.53×10^{-14}	5.53×10^{-14}	5.53×10^{-14}	5.53×10^{-14}

The results from each failure mode are discussed separately to indicate why redundancy does (or does not) improve system safety. Since the generator and motor failure probabilities are approximately the same order of magnitude, a nominal component failure rate, x, is defined for the remainder of the discussions in this section. The order of magnitude analysis performed in the following discussions is predicated on the assumption that each failure is a rare event ($x \ll 1$).

The analyses in the following discussions consider failures involving only generators or only motors. For some failure modes, it is possible that combinations of generators and motors could fail. However, these are less impactful on the system-level failure intensities and obfuscate the general findings of this work.

Some of the following discussions refer to the FAA's "quantitative probability terms" [21], which define how frequently a system-level failure may occur. These terms and corresponding probability bounds are listed in Tab. 8.

Table 8 Quantitative probability terms defined in FAA Advisory Circular 25.1309-1B.

Term	Lower Bound (/flight hour)	Upper Bound (/flight hour)
Probable	1×10^{-5}	1×10^{-3}
Remote	1×10^{-7}	1×10^{-5}
Extremely Remote	1×10^{-9}	1×10^{-7}
Extremely Improbable	—	1×10^{-9}

1. 1-EP Failure Scenario

On the baseline architecture, only one generator or motor must fail. Thus, the system-level failure probability is obtained by adding all component failure probabilities together:

$$16x + 4x = 20x$$

Once redundancy is added, multiple generators or a single motor must fail. Since the generator and motor component failure probabilities are nominally the same order of magnitude, a motor failure is much more likely to occur than multiple generator failures.

For example, in the Double Redundancy architecture, the failure mode is triggered by one of 16 possible motors failing, or one of two pairs of generators failing. Thus, the system-level failure probability is:

$$16x + 2x^2 \approx 16x$$

In summary, a single electric propulsor failure in the redundant propulsion system architectures is dominated by a motor failure. The likelihood of multiple generators failing is negligible relative to that of a single motor, explaining why there is minimal improvement as more redundancy is added for this failure mode.

2. 2-EP Failure Scenario

For two electric propulsors to fail on the baseline architecture, either one (of four) generators or two motors (of the 120 possible combinations) must fail. The system-level failure probability is:

$$120x^2 + 4x \approx 4x$$

Thus, for the baseline architecture, it is easier to fail one generator than it is to fail multiple motors. However, this is not true for the redundant architectures. In the Double Redundancy architecture, either one of the two redundant generator pairs or two of the motors must fail. The system-level failure probability is:

$$120x^2 + 2x^2 \approx 120x^2$$

Once redundancy is added, it becomes just as difficult to fail two generators as it does to fail two motors. As a result, the 120 possible motor failure combinations are more likely to occur. In the remaining redundant system architectures, the exponent on the second addend increases (corresponding to additional redundant connections between each generator and motor), making the contribution of the generator failures less significant, thus explaining the small system safety improvements observed.

3. 4-EP Failure Scenario

On the baseline architecture, a failure occurs if one of the generators fails or four of the motors fail (1,820 possible combinations). The system-level failure probability is approximately:

$$1,820x^4 + 4x \approx 4x$$

Since the generator failure modes are dominant, there is minimal safety improvement by adopting the 4-EP failure scenario relative to a 2-EP failure scenario. The minimal improvement comes from the requirement that four motors must fail instead of two.

In the redundant architectures, the generator failures remain more likely to occur than the motor failures. However, this trend changes once the Quadruple Redundancy configuration is considered. At this point, the system-level failure probability is approximately:

$$1,820x^4 + x^4 \approx 1,820x^4$$

The motor failures now dominate the expression because both failure modes require four components to fail. The thousands of possible motor failure combinations outweigh the likelihood of all four generators failing.

4. 8-EP Failure Scenario

For eight electric propulsors to fail on the baseline architecture, either two of the four generators (6 possible combinations) or eight motors (12,870 possible combinations) must fail. The nominal system-level failure probability is:

$$12,870x^8 + 6x^2 \approx 6x^2$$

which is dominated by the generator failures.

As redundancy is added to the system architecture, a similar behavior is observed as demonstrated in the 4-EP failure scenario; it is easier to fail multiple generators than it is to fail eight motors. For example, in the Quadruple Redundancy configuration, the nominal system-level failure probability is:

$$12,870x^8 + x^4 \approx x^4$$

highlighting how it is significantly more likely that all four generators fail than eight motors.

Additionally, this failure mode exhibits the most significant safety improvement between the Double Redundancy and Double In, Triple Out configurations (seven orders of magnitude improvement). To fail eight electric propulsors in the Double In, Triple Out configuration, all four generators must fail. This is due to the third redundant connection on the eight outboard motors (see Fig. 8 in Appendix V.C), which causes only six motors to fail if three generators fail. This system architecture leverages greater propulsion system redundancy to improve system safety at a limited performance cost (additional fuel burn).

5. 16-EP Failure Scenario

For all propulsion system architectures considered, either all four generators or all 16 motors must fail. Thus, the system-level failure probability is:

$$x^{16} + x^4 \approx x^4$$

and remains constant, regardless of the redundancy included in the system architecture. The likelihood of all four generators failing is always greater than that of all 16 motors failing. Although it is highly unlikely that this failure mode would be selected for certification, it suggests that there are no system safety benefits from adding redundant generator-motor connections.

C. Optimal System Architecture Selection

A Pareto Frontier was developed to assess the tradeoff between system-level performance and safety. Figure 6 plots the common logarithm of the system-level failure intensity against the fuel burn increase. The dashed lines on the plot represent the *upper bounds* of the FAA's quantitative probability terms [21].

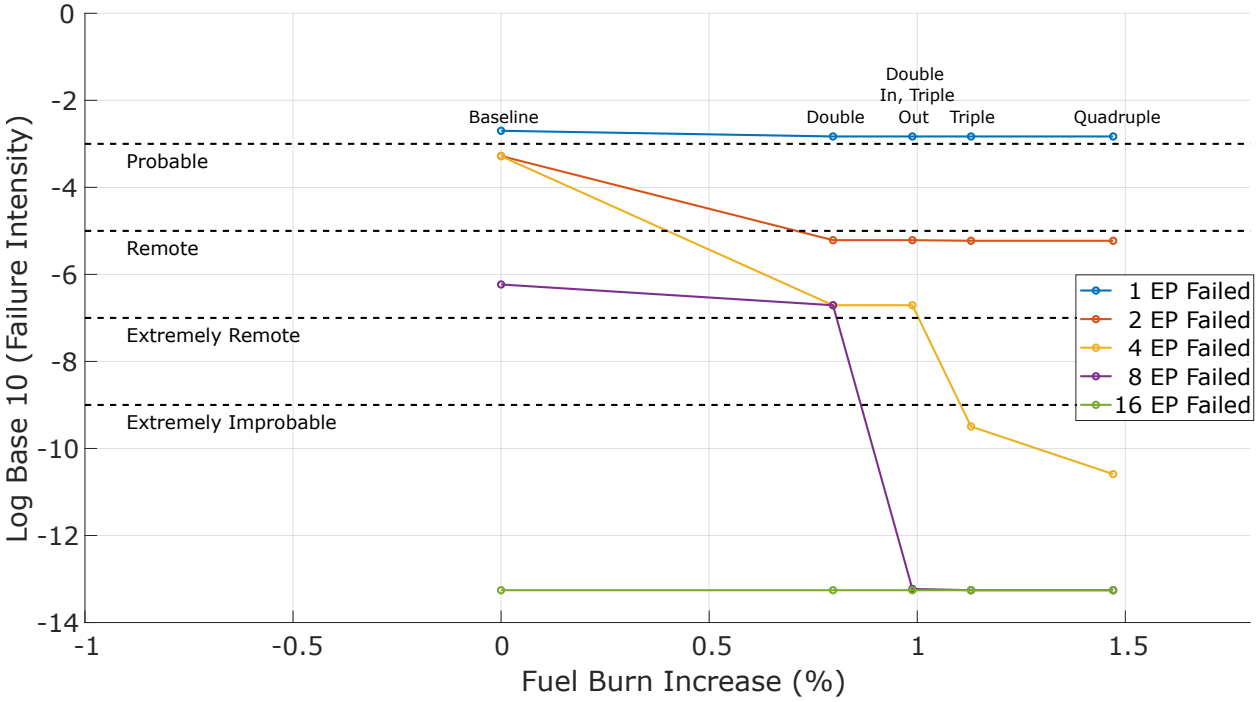

Fig. 6 Performance-reliability tradeoffs for different propulsion system architectures and failure modes. Points with the same fuel burn increase have the same propulsion system architecture (each labeled above the top line).

First, the tradeoffs between system-level performance and safety are examined. Then, optimal system architecture selection is discussed in the context of FAA Part 25.1309 [23], which delineates the permitted frequency and severity of system failures onboard an aircraft.

1. Performance-Safety Tradeoffs

The redundant system architectures improve system safety while requiring more fuel to fly the same mission. As redundant connections are included, additional cables are required to transmit power between the generators and motors, thus increasing the component-level weights.

Furthermore, the failure mode selected greatly affects whether the redundant configurations improve system safety or not. For a 1-EP failure scenario, the likelihood of a failure occurring is always greater than the "Probable" limits imposed by the FAA, regardless of the redundancy included in the propulsion system architecture. In contrast, there is no system safety improvement when adding redundancy under the 16-EP failure scenario; enough redundancy already exists with the four generators installed in the propulsion system.

There appears to be a reasonable compromise in improved system safety and performance penalties under the 4- and 8-EP failure scenarios. For the 4-EP failure scenario, a Triple Redundancy configuration ensures that the failure mode is "Extremely Improbable." The same safety level is achieved in the Double In, Triple Out configuration under the 8-EP failure scenario, even though the difference between failure probabilities is about five orders of magnitude; this is because no lower bound exists for the "Extremely Improbable" failure classification.

There are different system safety improvement gains depending on the failure mode selected. In a 4-EP failure scenario, increased redundancy gradually improves system safety. Each time a redundant connection is added (with exception to the Double In, Triple Out configuration), the system safety improves by multiple orders of magnitude. In contrast, under an 8-EP failure scenario, nearly all of the system safety improvements come from the additional connections provided by the Double In, Triple Out Redundancy configuration; there is minimal system safety improvement (if any at all) between the baseline and Double Redundancy configurations, and the Triple and Quadruple Redundancy configurations.

2. Optimal System Architecture Selection

Both system-level performance and safety must be considered while selecting an optimal system architecture. Prior safety discussions introduced the FAA's quantitative probability terms [21], but did not place them in the context of aircraft certification. To align with the certification criteria, these terms must be combined with the FAA's "failure condition classifications" – Minor, Major, Hazardous, and Catastrophic – which reflect the severity of the failure that occurred [24].

The acceptable frequency and severity of failures is defined by 14 CFR 25.1309(b) [23], stating that:

1) "Each catastrophic failure condition – (i) must be extremely improbable; and (ii) must not result from a single failure."
2) "Each hazardous failure condition must be extremely remote."
3) "Each major failure condition must be remote."

Although not definitively stated in the regulation, it is assumed that each minor failure condition must be probable.

To recommend optimal propulsion system architectures, the severity of each k-EP inoperative failure mode is classified based on the definitions provided in 14 CFR 25.4(b) [24]. Then, using the Pareto Frontier from Fig. 6, two optimal system architectures were identified: 1) one that minimizes fuel burn while achieving the requisite safety margin required by FAA Part 25.1309; and 2) one that significantly exceeds the requisite safety margin. These classifications and recommendations are outlined in Tab. 9.

Table 9 Failure mode classifications and Pareto-optimal propulsion system architectures selected.

Failure Mode	Classification	Pareto Optimum, Minimum Fuel	Pareto Optimum, Maximum Safety
1-EP	Minor	None	None
2-EP	Minor	Baseline	Double
4-EP	Major	Double	Triple
8-EP	Hazardous	Double In, Triple Out	Double In, Triple Out
16-EP	Catastrophic	Baseline	Baseline

The failure condition classification rationale is rooted in multiple considerations and assumptions. For SUSAN's wing-mounted distributed propulsors, a 4-EP failure is expected to cause a measurable performance decrement and

lateral trim changes while maintaining adequate controllability with moderate crew workload. Thus, it is classified as a *major* failure. An 8-EP failure – particularly when clustered – can require prompt crew action, degrade climb capability, and reduce control margin, warranting a *hazardous* classification. A 16-EP failure constitutes a *catastrophic* condition, putting the aircraft and its passengers in jeopardy. These classifications are configuration-specific and may be revised as higher-fidelity handling-quality analyses become available. *These classifications have been based on the authors' judgment, and may not reflect the actual classifications if an advanced concept like SUSAN were to be certified.* The reader may modify these classifications based on their expertise, possibly leading to different conclusions and recommendations than the ones made here.

Based on the Pareto Frontier and failure mode classifications, the optimal system architecture for both objectives varies depending on the failure mode selected. For the 2- and 4-EP failures, block fuel is minimized using the Baseline and Double Redundancy configurations, respectively. However, more redundant system architectures could be selected to maximize the safety margin (Double Redundancy for the 2-EP failure and Triple Redundancy for the 4-EP failure). For the 8- and 16-EP failures, there is no difference between the system architecture that minimizes fuel burn or significantly exceeds the safety margin.

V. Conclusions

NASA's SUSAN aircraft concept has been regarded as transformational, making the future of commercial flight more efficient. There have been limited quantitative studies on its propulsion system's reliability and safety. Furthermore, no prior literature explores the safety ramifications of introducing redundant connections within the electrified propulsion system; redundancy in the distributed propulsion system is assumed to be satisfactory, resulting in optimizations for performance and weight objectives only. To fill this gap, a performance-reliability framework was developed to assess the system-level performance and safety tradeoffs for SUSAN's baseline propulsion architecture and four propulsion system architectures that incorporate redundancy via additional generator-motor cross-connections.

The redundant connections between the generators/motors serve as a mechanism for trading system-level performance and safety objectives. The Pareto Frontier highlights that fuel burn is minimized by limiting redundant connections in the propulsion system, thus reducing the cable weight and size of the generators. In contrast, safety is maximized by adding redundant connections between the generators and motors in the propulsion system.

There are additional tradeoffs between redundancy in the system architecture and its dominant failure mode. The baseline configuration is most susceptible to a generator failure. However, depending on the failure mode selected, the redundant system architectures could fail from combinations of generator or motor failures.

Incorporating FAA Part 25.1309 safety regulations into the trade studies reveal that there are multiple Pareto-optimal system architectures depending on the engineer's primary objective. For the 2- and 4-EP failure modes, there are two possible Pareto-optimal system architectures – one that minimizes fuel burn while satisfying the requisite safety requirements, and one that significantly exceeds the safety margins. To minimize fuel burn, the Baseline (2-EP failure) or Double Redundancy (4-EP failure) configurations are optimal. To maximize safety, the Double (2-EP failure) or Triple Redundancy (4-EP failure) configurations are optimal. For the 8- and 16-EP failure modes, there is no difference between the configurations that minimize fuel burn and significantly exceed the safety margin; the optimal ones are the Double In, Triple Out (8-EP failure) or Baseline (16-EP failure). The predictions and recommendations made here are *based on the authors' judgment and experience*, and may differ from those of a subject matter expert. Future collaboration with such experts can help verify or modify the assumptions made in this study, thus confirming or refuting the optimal system architectures selected.

Furthermore, this study highlights the advantages of distributed electric propulsion systems from a safety perspective. The repeated propulsor units within the system act as a built-in redundancy, bolstering system safety while facilitating a more graceful degradation of the propulsion system's performance. However, depending on the failure mode selected for certification, this redundancy may not be enough to satisfactorily meet the stringent safety criteria. While this work proposed installing redundant connections between the generators and motors, additional redundancy could also be achieved by adding more propulsors to the distributed electric propulsion system. Tradeoffs between redundancy mechanisms and their impacts on the propulsion system weight/safety could be explored in future work.

Aside from the trade studies previously mentioned, there are three other ways to expand upon this work. First, the FTA assigned a single failure probability to each component. For further subsystem- and component-level studies, more detail can be added to the FTA by considering the possible failure modes within each component. Second, the component-level failure probabilities used in this study were scaled by applied environmental factors. As electrified aircraft technologies improve, these factors could be reduced or removed, resulting in improved system safety and

possibly new Pareto-optimal propulsion system architectures. Third, the Pareto-optimal system architectures, in combination with the FAA's failure condition classifications, could be utilized to select a primary propulsion system failure mode for SUSAN's propulsion system, paving a pathway for certification in the future.

Overall, this work establishes a strong foundation for justifying SUSAN's propulsion system design with both performance and safety objectives in mind.

Reproducibility and Data Availability: All performance and reliability results are reproducible from *publicly available archived input files*; see Ref. [25] for the open-access data. This data enables reproduction of the results generated in Tabs. 4, 6, and 7, and Fig. 5. Replicating these analyses requires specific versions of the FAST to be downloaded, which are available in Ref. [25] and on GitHub [*]. The earliest version of MATLAB tested with this code was Version R2019b.

Appendix

A. SUSAN Modeling Parameters

The parameters used to model SUSAN in FAST are listed in Tab. 10. Recall that, to simplify the propulsion system analysis, all parts of the electrified propulsion system (batteries, buses, circuit breakers, etc.) *excluding* the cables were removed from the propulsion system; their mass was accounted for in the "EAP Weight" group. To simplify the safety analysis, only generator and motor failures were considered; all other electrical components were assumed to be fully operational, as well as the turbofan engine and fans in the distributed propulsion system.

Table 10 Parameters to model SUSAN in FAST.

Parameter	Value	Units
Fuel Flow Calibration Factor	0.950	—
Airframe Calibration Factor	1.094	—
Entry into Service Year	2040	—
Passengers	190	—
Takeoff Speed	82.3	m/s
Cruise Speed	0.775	Mach
Cruise Altitude	11,278	m
Design Range	4,630	km
MTOW	86,586	kg
Wing Loading	634	kg/m^2
Fuel Weight	13,762	kg
EAP Weight	9,178	kg
Thrust-to-Weight Ratio	0.298	—

[*] https://github.com/ideas-um/FAST

B. Cable Lengths

Table 11 lists the cable lengths estimated from the digitized propulsion system schematic in Fig. 3.

Table 11 Estimated cable lengths (all in m).

	Generator 1	Generator 2	Generator 3	Generator 4
Motors 1/16	18.66	18.07	17.50	17.15
Motors 2/15	17.50	16.92	16.34	15.98
Motors 3/14	16.40	15.80	15.22	14.85
Motors 4/13	15.35	14.72	14.11	13.73
Motors 5/12	14.37	13.68	13.05	12.66
Motors 6/11	13.36	12.70	12.06	11.62
Motors 7/10	12.36	11.71	11.08	10.64
Motors 8/9	11.34	10.70	10.08	9.66

C. Redundant Propulsion Architectures

Figure 7 illustrates the Double Redundancy propulsion architecture. Each generator can provide power to eight motors. Each motor can receive power from two generators.

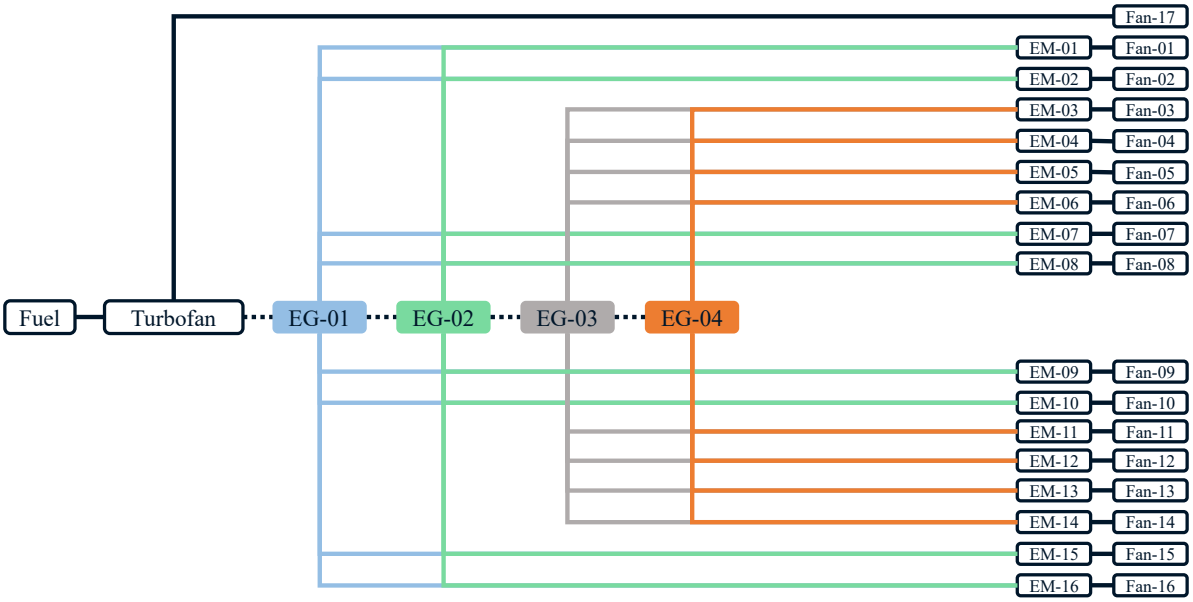

Fig. 7 Double Redundancy propulsion architecture.

Figure 8 illustrates the Double Inboard, Triple Outboard propulsion architecture. Each generator can provide power to ten motors. The outboard motors (1-4, 13-16) can receive power from three generators. The inboard motors (5-12) can receive power from two generators.

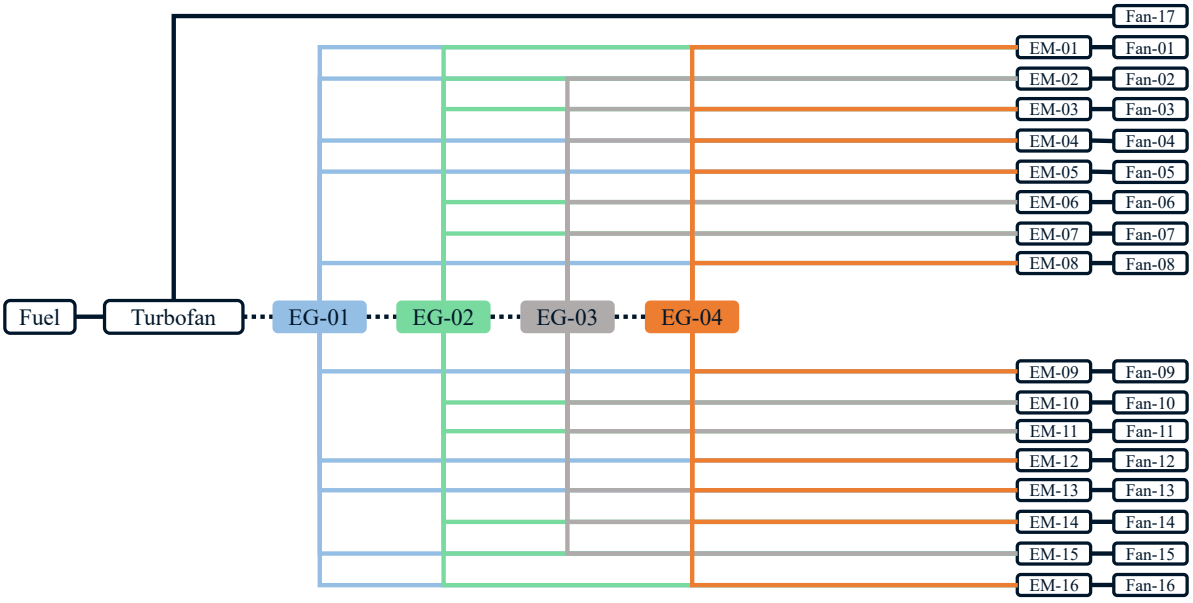

Fig. 8 Double Inboard, Triple Outboard propulsion architecture.

Figure 9 illustrates the Triple Redundancy propulsion architecture. Each generator can provide power up to 12 motors. Each motor can receive power from three generators.

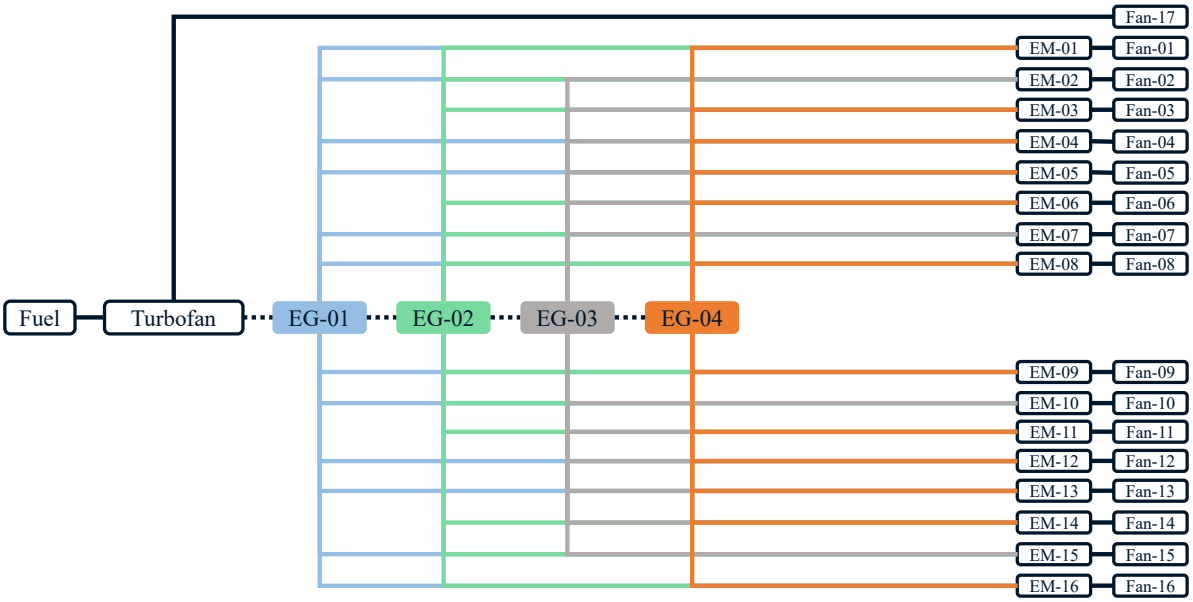

Fig. 9 Triple Redundancy propulsion architecture.

Figure 10 illustrates the Quadruple Redundancy propulsion architecture. Each generator can provide power to all 16 motors. Each motor can receive power from all four generators.

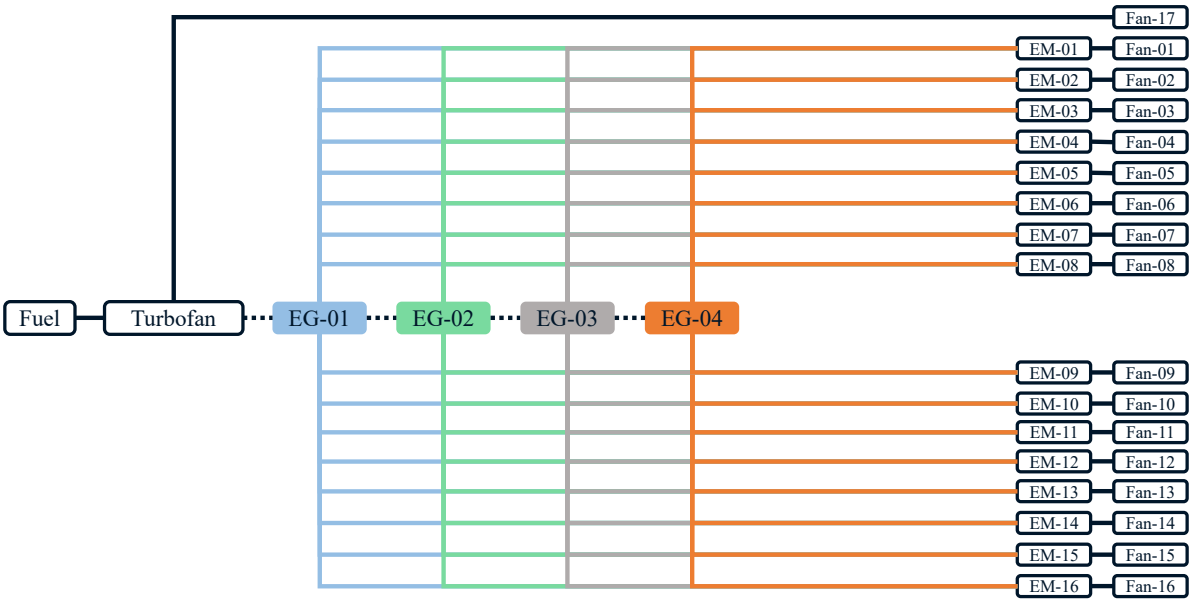

Fig. 10 Quadruple Redundancy propulsion architecture.

Funding Sources

This work is sponsored by the NASA Aeronautics Research Mission Directorate and Electrified Powertrain Flight Demonstration project, "Development of a Parametrically Driven Electrified Aircraft Design and Optimization Tool", Glenn Engineering and Research Support Contract (GEARS) Contract WO-0238.

Acknowledgments

The authors would like to thank Amy Chicatelli, Karin Bozak, Nolan LaMarche, and Ralph Jansen from NASA's Electrified Powertrain Flight Demonstration project for supporting this work and providing valuable technical input and feedback throughout the duration of the project.

References

[1] National Aeronautics and Space Administration, "Electrified Aircraft Propulsion," , 2024. URL `https://www1.grc.nasa.gov/aeronautics/eap/`.

[2] Chau, T., and Duensing, J., "Conceptual Design of the Hybrid-Electric Subsonic Single Aft Engine (SUSAN) Electrofan Transport Aircraft," *AIAA SciTech 2024 Forum*, 2024, p. 1326. https://doi.org/10.2514/6.2024-1326.

[3] Chau, T., Kenway, G., and Kiris, C. C., "Conceptual Exploration of Aircraft Configurations for the SUSAN Electrofan," *AIAA SciTech 2022 Forum*, 2022, p. 2181. https://doi.org/10.2514/6.2022-2181.

[4] Jansen, R., Kiris, C. C., Chau, T., Machado, L. M., Duensing, J. C., Mirhashemi, A., Chapman, J., French, B. D., Miller, L., Litt, J. S., et al., "Subsonic Single Aft Engine (SUSAN) Transport Aircraft Concept and Trade Space Exploration," *AIAA SciTech 2022 Forum*, 2022, p. 2179. https://doi.org/10.2514/6.2022-2179.

[5] Mirhashemi, A., Chapman, J., Miller, C., Julia, S., and Jansen, R., "Tail-Mounted Engine Architecture and Design for the Subsonic Single Aft Engine Electrofan Aircraft," *AIAA SciTech 2022 Forum*, 2022, p. 2182. https://doi.org/10.2514/6.2022-2182.

[6] Machado, L. M., Chau, T., Kenway, G. K., Duensing, J. C., and Kiris, C. C., "High-Fidelity Aerodynamic Analysis and Optimization of the SUSAN Electrofan Concept," *AIAA SciTech 2022 Forum*, 2022, p. 2304. https://doi.org/10.2514/6.2022-2304.

[7] Heersema, N., and Jansen, R., "Thermal Management System Trade Study for SUSAN Electrofan Aircraft," *AIAA SciTech 2022 Forum*, 2022, p. 2302. https://doi.org/10.2514/6.2022-2302.

[8] Haglage, J., Dever, T., Jansen, R., and Lewis, M., "Electrical System Trade Study for SUSAN Electrofan Concept Vehicle," *AIAA SciTech 2022 Forum*, 2022, p. 2183. https://doi.org/10.2514/6.2022-2183.

[9] Lynde, M. N., Campbell, R. L., and Hiller, B. R., "A Design Exploration of Natural Laminar Flow Applications for the SUSAN Electrofan Concept," *AIAA Scitech 2022 Forum*, 2022, p. 2303. https://doi.org/10.2514/6.2022-2303.

[10] Machado, L. M., Chau, T., Kenway, G. K., Duensing, J. C., and Kiris, C. C., "Preliminary Assessment of a Distributed Electric Propulsion System for the SUSAN Electrofan," *AIAA SciTech 2023 Forum*, 2023, p. 1748. https://doi.org/10.2514/6.2023-1748.

[11] Denham, C. L., and Jansen, R., "Initial Regulatory and Certification Approach for the SUSAN Electrofan Concept," *AIAA SciTech 2022 Forum*, 2022, p. 2180. https://doi.org/10.2514/6.2022-2180.

[12] Denham, C. L., Chau, T., Ryan, W., and Jansen, R., "Mission Profiles for the SUSAN Electrofan Concept," *AIAA SciTech 2023 Forum*, 2023, p. 1938. https://doi.org/10.2514/6.2023-1938.

[13] National Archives and Records Administration, "Definitions (14 CFR 25)," , 2025. URL https://www.ecfr.gov/current/title-14/chapter-I/subchapter-C/part-25.

[14] Mokotoff, P. R., Arnson, M., Wang, Y.-C., and Cinar, G., "FAST: A Future Aircraft Sizing Tool for Conventional and Electrified Aircraft Design," *Journal of Aircraft*, 2025, pp. 1–18. https://doi.org/10.2514/1.C038452.

[15] Mokotoff, P. R., and Cinar, G., "A Graph-based Framework for Advanced Aircraft Propulsion System Analysis," *Aerospace Science and Technology*, 2025, p. 110798. https://doi.org/10.1016/j.ast.2025.110798.

[16] Wang, Y.-C., Stockhausen, M., Mokotoff, P. R., Arnson, M. G., and Cinar, G., "SUbsonic Single Aft eNgine (SUSAN) System Integration Analysis With the Future Aircraft Sizing Tool (FAST)," *AIAA SciTech 2025 Forum*, 2025, p. 2376. https://doi.org/10.2514/6.2025-2376.

[17] Chapman, J. W., Kratz, J. L., Dever, T., Mirhashemi, A., Heersema, N., and Jansen, R., "SUSAN Concept Vehicle Power and Propulsion System Study," *AIAA SciTech 2023 Forum*, 2023, p. 1749. https://doi.org/10.2514/6.2023-1749.

[18] Society of Automotive Engineers, "Guidelines for Conducting the Safety Assessment Processon Civil Aircraft, Systems, and Equipment," Tech. rep., Society of Automotive Engineers, 2023. ARP4761A.

[19] Limnios, N., *Fault Trees*, John Wiley & Sons, 2013.

[20] Darmstadt, P. R., Catanese, R., Beiderman, A., Dones, F., Chen, E., Mistry, M. P., Babie, B., Beckman, M., and Preator, R., "Hazards Analysis and Failure Modes and Effects Criticality Analysis (FMECA) of Four Concept Vehicle Propulsion Systems," Tech. rep., National Aeronautics and Space Administration, 2019. URL https://ntrs.nasa.gov/citations/20190026443.

[21] Federal Aviation Administration, "System Design and Analysis (AC 25.1309-1B)," , 2024. URL https://www.faa.gov/regulations_policies/advisory_circulars/index.cfm/go/document.information/documentID/1043037.

[22] Vesely, W. E., Goldberg, F. F., Roberts, N. H., and Haasl, D. F., "Fault Tree Handbook," Tech. rep., U.S. Nuclear Regulatory Commission, 1981. NUREG-0492.

[23] National Archives and Records Administration, "Equipment, Systems, and Installations (14 CFR 25.1309)," , 2025. URL https://www.ecfr.gov/current/title-14/chapter-I/subchapter-C/part-25/subpart-F/subject-group-ECFR9f24bf451b0d2b1/section-25.1309.

[24] National Archives and Records Administration, "Definitions (14 CFR 25.4)," , 2025. URL https://www.ecfr.gov/current/title-14/chapter-I/subchapter-C/part-25/subpart-A/section-25.4.

[25] Mokotoff, P. R., and Cinar, G., "Reliability and Performance Trade Studies for NASA's Subsonic Single Aft Engine Aircraft," , 2025. https://doi.org/10.7302/wg2f-nv21, Data Set.